High-throughput photocapture approach for reaction discovery

Alison A. Bayly[a], Benjamin R. McDonald[a], Milan Mrksich[a,1], and Karl A. Scheidt[a,1]

[a]Department of Chemistry, Northwestern University, Evanston, IL 60208

Edited by Alexis T. Bell, University of California, Berkeley, CA, and approved April 29, 2020 (received for review February 21, 2020)

Modern organic reaction discovery and development relies on the rapid assessment of large arrays of hypothesis-driven experiments. The time-intensive nature of reaction analysis presents the greatest practical barrier for the execution of this iterative process that underpins the development of new bioactive agents. Toward addressing this critical bottleneck, we report herein a high-throughput analysis (HTA) method of reaction mixtures by photocapture on a 384-spot diazirine-terminated self-assembled monolayer, and self-assembled monolayers for matrix-assisted laser desorption/ionization mass spectrometry (SAMDI-MS) analysis. This analytical platform has been applied to the identification of a single-electron-promoted reductive coupling of acyl azolium species.

high-throughput analysis | self-assembled monolayers | photocapture | azoliums

The development of new carbon–carbon bond forming reactions underpins progress in the development of pharmaceutical and agrochemical agents. Over the past decade numerous reports detailing new reactivity through N-heterocyclic carbene (NHC) organocatalysis have been published (1) While these carbene catalysis manifolds have clearly been broadly explored, significant opportunities remain. The traditional two-electron NHC reactivity has defined the electrophile scope to mainly activated π-acceptors such as carbonyl and imine-containing compounds. Consequently, even straightforward reactions, such as alkylations, remain largely unrealized. However, distinct single-electron strategies with NHC catalysis and the associated acyl azolium intermediates could open new pathways by engaging reactive partners outside the traditional π-acceptors mentioned above.

Redox NHC/azolium-based transformations have largely focused on oxidation of NHC intermediates, resulting in various transformations of aldehydes to acids or esters (2–4). Early work from the Scheidt laboratory achieved the oxidation of the Breslow intermediate for the esterification of aldehydes (Fig. 1*A*) (2). In another significant report, Boydston and coworkers demonstrated that the Breslow intermediate can be oxidized under electrochemical conditions (Fig. 1*B*) (3). Studer and coworkers later demonstrated that the electrochemical apparatus could be substituted with a ruthenium catalyst and air (Fig. 1*B*) (4). Outside of these oxidations of the Breslow intermediate, there are limited examples of single-electron oxidative NHC/azolium manifolds involving either homoenolates (5) or decarboxylative couplings (6, 7).

We hypothesized that a useful and unique radical intermediate could be accessed via the single-electron reduction of acyl azolium species (Fig. 1*C*). While the redox chemistry of azolium salts has been investigated (8), the potential of acyl azolium salts under these conditions has not. The reduction potential of azoliums spans a wide range (–1.3 to –2.2 V) (8). Importantly, these values establish azoliums as reducible by commonly used photoredox catalysts. Accordingly, the reduction of acylated variants should be more facile. We envisioned that a photoredox catalyst could reduce an acyl azolium, with the restoration of azolium aromaticity driving the radical to carbonyl carbon. In conjunction with this mesomeric stabilization, the flanking *N*-methyl groups could provide steric shielding, leading to persistent ketyl radicals (9) that would couple with benzyl radical species to form ketones, highly valuable synthetic moieties (Fig. 1*C*). To efficiently evaluate our hypothesis, we sought to screen different potential ketyl-type radical precursors (10, 11), alkyl radical precursors (9, 12), Lewis acid additives (13–15), and solvents. With a daunting array of variables to investigate, we searched for methods to rapidly survey this broad chemical space.

Typically, high-throughput screens are analyzed via conventional methods such as ultraperformance liquid chromatography mass spectrometry (UPLC-MS), or gas chromatography mass spectrometry (GC-MS) (16–19) Although these approaches can be effective, long analysis times limit screening efficiency. Specifically, most conventional UPLC-MS and GC-MS instruments typically require 5–6 h and 10–12 h with conventional sample run times, respectively, to process a 96-well sample plate.

To alleviate this analytical bottleneck, we looked to surface analytical techniques, which in recent years have demonstrated remarkable high-throughput capabilities (20–22). Specifically, the surface analytical technique self-assembled monolayers for matrix-assisted laser desorption/ionization mass spectrometry (SAMDI-MS) provides a general method for performing high-throughput experiments (23, 24). Self-assembled monolayers (SAMs) are well-defined structures formed by spontaneous assembly of functionalized alkanethiols on a gold-coated substrate (Fig. 2*A*) (25). Monolayers can be functionalized with a broad range of molecular groups and then treated with reagents (or enzymes) to yield products that are efficiently analyzed by SAMDI-MS (23, 24). Much of our previous work has performed reactions directly on the

Significance

Mass spectrometry (MS) has inspired powerful modes of reaction discovery. Chemists often rely on MS methods, such as liquid-chromatography MS and gas chromatography MS, to rapidly assess hundreds of small-scale reactions. These chromatography-based MS techniques are preferred as they typically provide data consistent with scaled-up yields. Other MS approaches that more rapidly analyze reactions frequently provide results inconsistent with scaled-up yields. Herein we describe the development of a high-throughput platform that overcomes the analytical bottleneck presented by chromatography-based MS techniques while retaining consistency with scaled-up results. Our MS method, which combines diazirine photocapture and self-assembled monolayers for desorption/ionization MS, enabled the analysis of ∼2,000 reactions in <2.5 h to realize an intermolecular photoredox reaction.

Author contributions: A.A.B., B.R.M., M.M., and K.A.S. designed research; A.A.B. performed research; M.M. and K.A.S. analyzed data; and A.A.B., M.M., and K.A.S. wrote the paper.

The authors declare no competing interest.

This article is a PNAS Direct Submission.

[1]To whom correspondence may be addressed. Email: milan.mrksich@northwestern.edu or scheidt@northwestern.edu.

This article contains supporting information online at https://www.pnas.org/lookup/suppl/doi:10.1073/pnas.2003347117/-/DCSupplemental.

First published June 1, 2020.

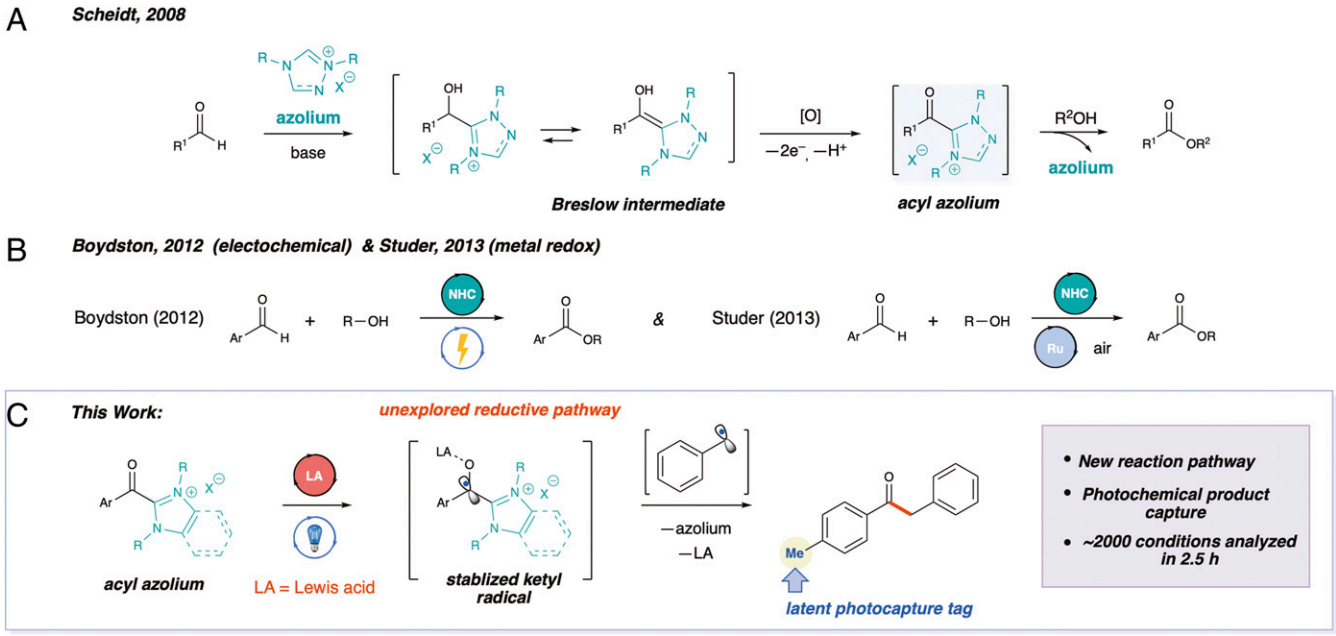

Fig. 1. Approaches to single-electron chemistry with NHC intermediates. (*A*) Initial investigation into oxidation of Breslow intermediate. (*B*) Electrochemical and metal-redox oxidation of NHC intermediates. (*C*) Reaction design plan for the reductive coupling of a ketyl radical with a benzyl (1°) radical to form a ketone.

immobilized molecules for simplicity, but with the consequence that reactivity on the monolayers did not always match the reactivity in solution (26, 27).

To circumvent this significant barrier while leveraging the efficient analysis times (~5 s per reaction), we implemented an approach where the reactions are performed in solution (using 96-well plates), followed by pipetting the reaction mixtures onto a diazirine-terminated SAM for UV-induced photocapture, and SAMDI-MS analysis (Fig. 2*A*). This method, termed traceless immobilization SAMDI-MS (TI-SAMDI-MS), has been applied as a tool to characterize a P450 drug-metabolizing enzyme and to monitor a Suzuki–Miyaura reaction (28); however, this method has never been applied to high-throughput analysis (HTA) until this work.

Results and Discussion

To validate our approach, we demonstrated that the authentic product could successfully immobilize to the diazirine monolayer and that this molecule could be observed via SAMDI-MS at *m*/*z* of 1,536 (Fig. 2*B*). With this process validated, we could investigate our hypothesized reactivity using the TI-SAMDI-MS analysis method (Fig. 2*C*).

Prior to our screen, we prepared two simple salts (**E1** and **E2**) to assess the reactivity of the acyl azolium NHC intermediate. We also incorporated six other electrophilic acyl sources (**E3**–**E8**) to determine necessity of the acyl azolium for the desired ketyl radical formation (Fig. 2*D*). Li and coworkers' impressive visible-light induced alkyl transfer report motivated us to incorporate the benzyl *t*-Bu Hantzsch ester (**Bn HEH**, $E_{1/2}$ = +1.08 V vs.) as a benzyl radical precursor substrate (Fig. 2*D*) (29). Additionally, Molander and coworkers' alkyl silicate developments and applications inspired us to include the alkyl radical precursor ammonium benzyl bis(catecholato)silicate (Bn Si, $E_{1/2}$ = +0.70 V vs. saturated calomel electrode [SCE]) (30). As commercially available carboxylic acids represent the ultimate radical precursor, we also included phenyl acetic acid (**Bn-COOH**) with an equimolar amount of base (Cs_2CO_3) as the third alkyl radical precursor (31). The ubiquity of Lewis acids in ketyl radical formation necessitated the investigation of various Lewis acids as additives (13–15).

Given the mechanistic duality in photoredox transformations (32–35) (reductive or oxidative photocatalyst-quenching cycles), we selected catalysts with a sufficiently broad redox potential range. Therefore, the first catalyst selected was the versatile metal polypyridyl complex $Ir(ppy)_2(dtbppy)PF_6$ (**PC 1**) ($E_{1/2}$ (Ir(III)*/Ir(II)) = +0.66 V vs. SCE and $E_{1/2}$ (Ir(III)*/Ir(IV)) = –0.96 V vs. SCE) (36). The organophotocatalyst 4CzIPN (**PC 2**) was also selected because we were interested in developing an inexpensive and metal-free approach. Given that it is easily accessible synthetically, and has a wide redox potential range ($E_{1/2}$ PC^*/PC^- = +1.35 V vs. SCE and $E_{1/2}$ PC^-/PC = –1.21 V vs. SCE), 4CzIPN was an ideal choice (37). Dimethylsulfoxide (DMSO) and MeCN were selected as the two solvents to be tested as they have been established as ideal solvents for charge-transfer reactions, and therefore are commonly implemented in synthetic photoredox chemistries (38).

With these eight electrophilic acyl sources, five Lewis acids, four Lewis acid loadings, three alkyl radical precursors, two photocatalysts (Ir-based catalyst and an organic-based catalyst), and two solvents, we set out to rapidly assess the various conditions (Fig. 2*D*). Under inert atmosphere, 1,920 total reactions were set up in 96-well photoredox plates and permitted to stir for 18 h on blue light emitting diode (LED) array pads (*SI Appendix*, Figs. S1 and S2). We set up four 96-well plates at one time in glovebox (1 h), then permitted the reactions to run overnight (12 h). Upon completion, the unpurified and unprocessed mixtures were pipetted directly onto the diazirine monolayer with a multichannel pipetter (15-min/384-spot plate), UV-irradiated, and analyzed via SAMDI-MS (Fig. 2*C*). Postdata acquisition the spectra were analyzed via our Applied Biosystems Data Explorer Software.

Impressively, this method analyzed 1,920 reactions in ~2.5 h (see *SI Appendix* for experimental details and all screening results). By this analysis, only six hits were found, constituting 0.3% of the reactions screened (Fig. 3*A*). Hit reactions were designated simply by whether the product peak (*m*/*z* of 1,536) was clear and strong enough that it could not be confused with spectral noise. We screened the limit of detection (LOD) and found that the product peak is not visible for yields of 30% or lower, and this

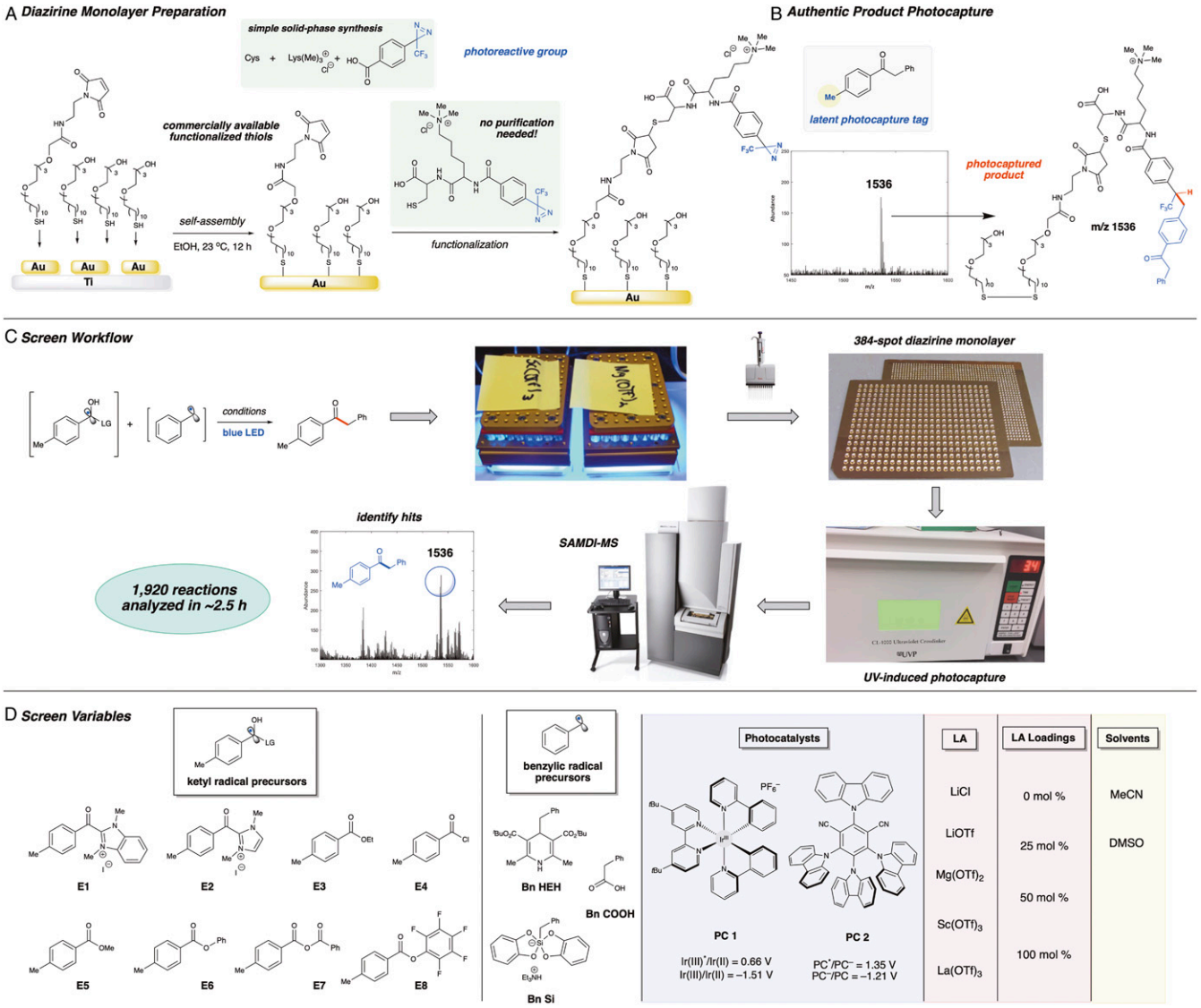

Fig. 2. (*A*) Diazirine monolayer preparation. (*B*) Authentic product photocapture. (*C*) Screen workflow. (*D*) Screen parameters.

peak is clearly observed for yields of 40% or higher (*SI Appendix*, Fig. S8). This LOD can be attributed to the photolyzed diazirine's highly reactive nature and its ability to insert readily into most molecules. The diazirine monolayer effectively reacts completely with the unpurified reaction mixture upon irradiation, and it is therefore unsurprising that several peaks are observed in addition to the product insertion peak. Although the LOD is higher than ideal, most reaction development programs would not pursue reactions below this ∼30% yield. Consequently, this LOD can be viewed as advantageous for robust reaction development. Efforts are underway to evaluate this platform's LOD for various reaction types.

The hit reactions were scaled to validate our findings and determine if these provided suitable yields (Fig. 3). The hit-reaction yields ranged from moderate (40%) to high (70%). The higher yields were consistent with the higher intensity SAMDI-MS peaks relative to other mixture components captured, and the moderate yields corresponded to the lower relative intensity peaks (Fig. 3*B*). Given the inconsistencies that often occur between matrix-assisted laser desorption/ionization (MALDI-MS) high-throughput screen outputs and UPLC or scaled-up results (22, 24) we ran 10 different scaled-up reactions with nonhit conditions (*SI Appendix*, Table S1). No false negatives were observed. Only three sets of reaction conditions resulted in any product conversion (see *SI Appendix*, Table S1 entries 1, 3, and 4); however, the isolated yields were below the LOD (30–40% yield). These data (Fig. 3 and *SI Appendix*, Table S1) establish that our screening platform identifies valid hits as long as the yields are above the limit of detection.

Li and coworkers' mechanistic insights for light-induced photoredox alkyl transfer with the Hantzsch ester (**Bn HEH**) heavily informs our proposed reaction pathway in Fig. 4 (29). Additionally, TEMPO, a radical scavenger, was applied to the best hit conditions and no product was observed, indicating that radical intermediates are involved (*SI Appendix*, Fig. S9). To better understand the radical intermediate, cyclic voltammetry (CV) measurements were performed on the acyl benzimidazolium salt (**E1**, Fig. 4*B*). Smooth, reversible electron transfer was observed for this substrate, indicating that the ketyl radical intermediate is stable until introduced to the benzyl radical for coupling (Fig. 4*A*). We were also pleased to observe that this reaction could be applied with two other benzyl Hantzsch esters on hand (**Br-Bn HEH** and **F-Bn HEH**) with moderate yields (Fig. 4*C*). Efforts are

A **Scaled-up hit reactions**

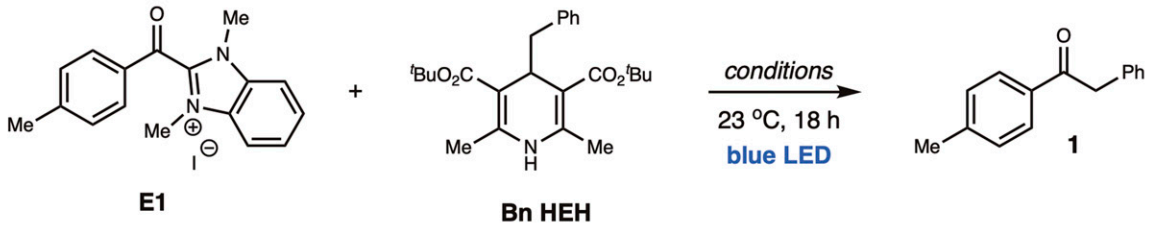

Hit entry	Photocatalyst	Lewis Acid	Solvent	Yield 1 (%)
1.	PC 1	LiCl (1.0 equiv)	MeCN	70
2.	PC 1	LiCl (1.0 equiv)	DMSO	53
3.	PC 1	LiOTf (0.25 equiv)	DMSO	40
4.	PC 1	none	MeCN	41
5.	PC 1	none	DMSO	65
6.	PC 2	LiCl (1.0 equiv)	MeCN	51

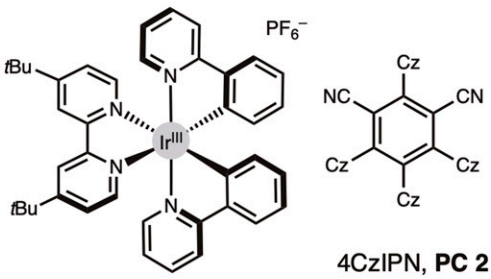

B **Hit spectra for entries 1–6**

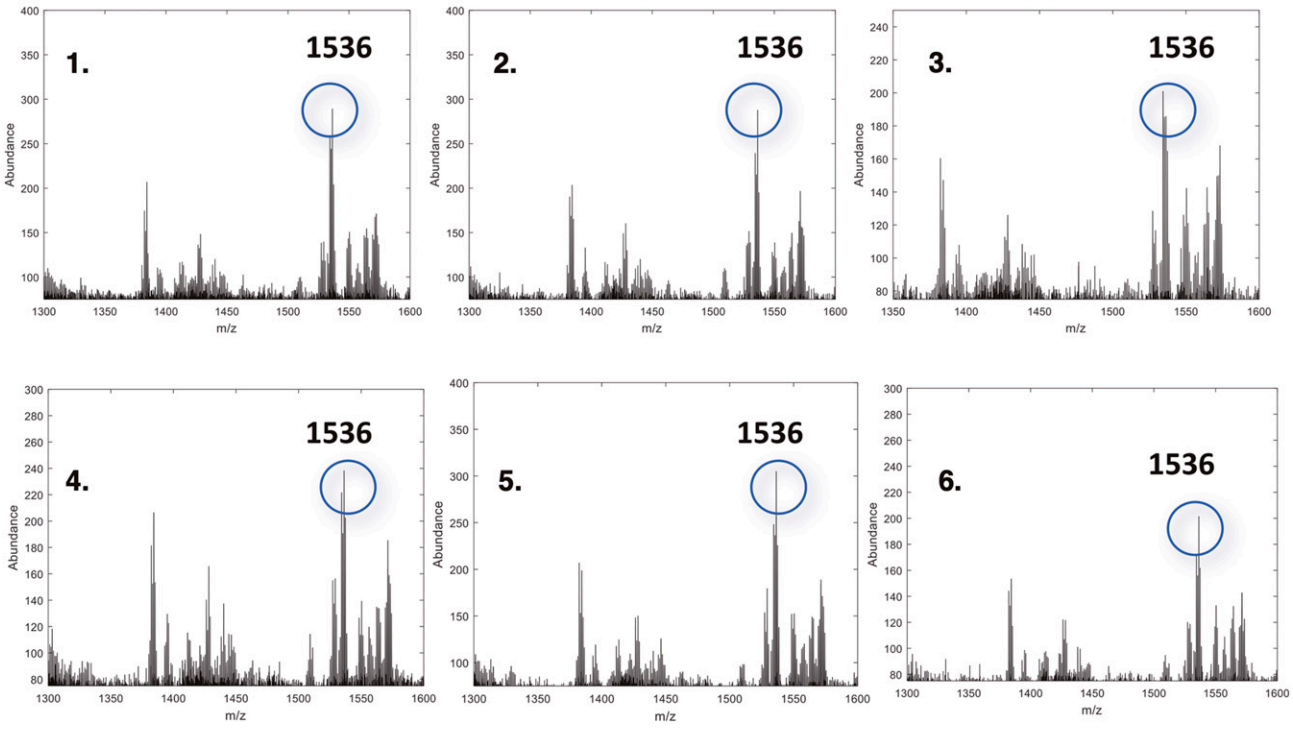

Fig. 3. (*A*) Scaled-up hit reactions (0.1 mmol **E1**, 0.15 mmol **Bn HEH**). (*B*) Hit spectra for entries 1–6.

currently underway to investigate the scope of this reaction further.

Conclusion

In conclusion, this work demonstrates an HTA that allowed us to efficiently and extensively evaluate an intermolecular carbon-carbon bond forming reaction. With regard to the technology developed, previous MALDI-based high-throughput platforms rely on ionizable functional groups built into the substrates involved in the reactions investigated. Our ionizable functional group (positively charged trimethyllysine) was built into the monolayer; therefore, it does not interfere with the reactions, but aids analysis. Moreover, given that we do not have to build our reaction around ionizable groups since ours is incorporated in

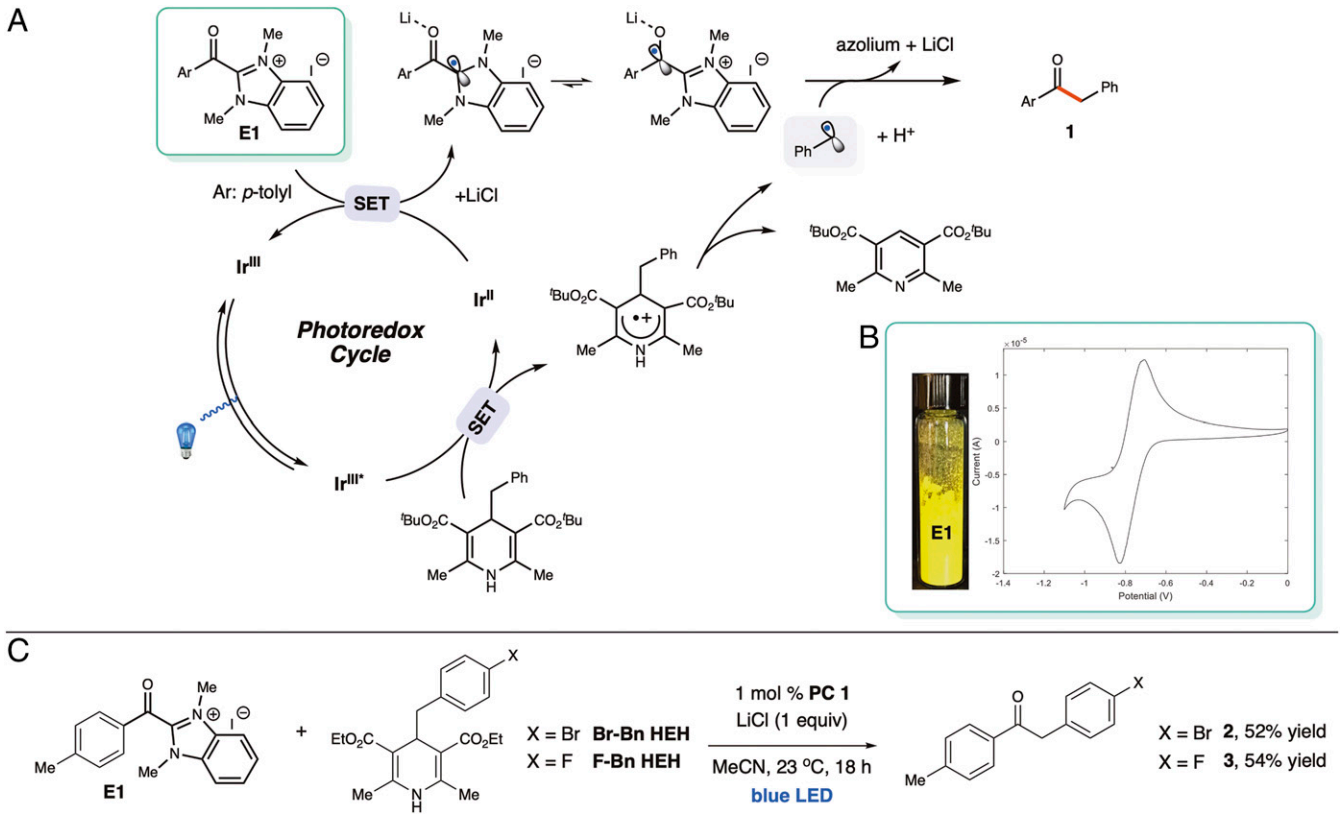

Fig. 4. (*A*) Proposed reaction pathway. (*B*) CV data for acyl benzimidazolium salt (**E1**). (*C*) Further examples with different Bn HEHs.

the SAM, TI-SAMDI-MS can be applied generally to any reaction. What distinguishes this platform most from other matrix-assisted laser desorption/ionization time of flight (MALDI-TOF)–based high-throughput methods is that for our approach the screen results consistently match the scaled-up or UPLC results. Such reliability is especially significant given that inconsistency between screen results and UPLC or scaled-up results has been a persistent problem with MALDI-MS analytical technology (22). The TI-SAMDI-MS platform overcomes this inconsistency issue while retaining the rapid analytics that MALDI-MS provides.

Our screen clearly and rapidly established that the acyl benzimidazolium salt (**E1**) was the superior ketyl radical precursor, and that the Hantzsch ester (**Bn HEH**) was the optimal alkyl radical precursor. This method also allowed us to identify specific nonobvious hit conditions (stoichiometric LiCl in MeCN) to achieve 70% yields. This transformation discovered via TI-SAMDI-MS is fundamental, and more broadly, the implications of both the HTA and this chemical discovery are significant. With nearly 2,000 reactions evaluated in ∼2.5 h, this semiquantitative analysis platform offers enormous value to reaction development programs. Importantly, the photogenerated carbene C-H insertion capture process enables the use of simple, nonelectronic or sterically biasing label, a benzylic methyl group. Finally, the radical–radical coupling discovered offers an intriguing strategy to form carbon-carbon bonds.

Materials and Methods

Diazirine SAMDI-Array Plate Preparation. Steel plates formatted to 384 wells coated with titanium (5 nm) and patterned with gold (30 nm) were soaked (18 h) in an ethanolic solution of tri(ethylene glycol)-alkanethiol (EG3-alkanethiol) disulfide and a mixed disulfide of EG3-alkanethiol and maleimide-terminated EG3-alkanethiol (0.1 mM). The arrays were subsequently washed with EtOH, deionized ultrafiltered (DIUF) H_2O, EtOH again, and dried under a stream of N_2. The photoaffinity linker solution (1 μM in Tris buffer, pH 8) was applied to the plates (1 μL per spot) and warmed to 37 °C for 30 min. Upon completion, the diazirine monolayer plate was washed with ethanol, DIUF H_2O, EtOH again, and dried under a stream of N_2.

Photoredox Reactions. Reactions were run in oven-dried glass vials in ParaDox 96-well-plate reactor blocks. The 96-well plates were brought into the glovebox and the four reaction components were added as stock solutions using micropipettes. The plates were sealed with screwed top lids equipped with polytetrafluoroethylene (PTFE) gaskets, removed from the glovebox, and placed on Lumidox 96-Well Blue LED arrays atop a magnetic stirrer (500 rpm). After 18 h, the plates were unsealed for analysis.

Reaction Photoimmobilization. Upon photoredox reaction completion, crude reaction mixture aliquots (1 μL from four 96-well plates) were directly pipetted onto the 384 diazirine monolayer spots. The 384-spot plate was then placed inside a UVP Cross-linker 1000L and irradiated (10 min, λ= 365 nm).

SAMDI Data Analysis. After reaction photoimmobilization, the array plates were washed (DIUF, then EtOH), treated with 2,4,6-trihydroxyacetophenone matrix (20 mg/mL in acetone), and dried using a stream of N_2. SAMDI arrays were analyzed via MALDI-TOF MS using an AB Sciex 5800 series instrument with 20-kV accelerating voltage in positive reflector mode (200 laser shots to each spot). The obtained spectra were analyzed in an automated fashion using the Applied Biosystems Data Explorer Software.

Data Availability. See *SI Appendix* for experimental details, spectra, and screening results.

ACKNOWLEDGMENTS. We thank the US Defense Advanced Research Projects Agency for generous support under the "Make-It" Award, 69461-CH-DRP W911NF1610384 and National Institute of General Medical Sciences (NIGMS) (R01GM073072, R01 GM131431, and F31GM116532 to B.R.M) for financial support.

1. M. N. Hopkinson, C. Richter, M. Schedler, F. Glorius, An overview of *N*-heterocyclic carbenes. *Nature* **510**, 485–496 (2014).
2. B. E. Maki, K. A. Scheidt, N-heterocyclic carbene-catalyzed oxidation of unactivated aldehydes to esters. *Org. Lett.* **10**, 4331–4334 (2008).
3. E. E. Finney, K. A. Ogawa, A. J. Boydston, Organocatalyzed anodic oxidation of aldehydes. *J. Am. Chem. Soc.* **134**, 12374–12377 (2012).
4. J. Zhao, C. Mück-Lichtenfeld, A. Studer, Cooperative *N*-heterocyclic carbene (NHC) and ruthenium redox catalysis: Oxidative esterification of aldehydes with air as the terminal oxidant. *Adv. Synth. Catal.* **355**, 1098–1106 (2013).
5. Y. Zhang *et al*., *N*-heterocyclic carbene-catalyzed radical reactions for highly enantioselective β-hydroxylation of enals. *J. Am. Chem. Soc.* **137**, 2416–2419 (2015).
6. T. Ishii, Y. Kakeno, K. Nagao, H. Ohmiya, *N*-heterocyclic carbene-catalyzed decarboxylative alkylation of aldehydes. *J. Am. Chem. Soc.* **141**, 3854–3858 (2019).
7. T. Ishii, K. Ota, K. Nagao, H. Ohmiya, *N*-heterocyclic carbene-catalyzed radical relay enabling vicinal alkylacylation of alkenes. *J. Am. Chem. Soc.* **141**, 14073–14077 (2019).
8. K. A. Ogawa, A. J. Boydston, Electrochemical characterization of azolium salts. *Chem. Lett.* **43**, 907–909 (2014).
9. D. Leifert, A. Studer, The persistent radical effect in organic synthesis. *Angew. Chem. Int. Ed. Engl.* **59**, 74–108 (2020).
10. A. Banerjee, Z. Lei, M. Y. Ngai, Acyl radical chemistry *via* visible-light photoredox catalysis. *Synthesis (Stuttg)* **51**, 303–333 (2019).
11. C. Raviola, S. Protti, D. Ravelli, M. Fagnoni, Photogenerated acyl/alkoxycarbonyl/carbamoyl radicals for sustainable synthesis. *Green Chem.* **21**, 748–764 (2019).
12. H. Fischer, The persistent radical effect: A principle for selective radical reactions and living radical polymerizations. *Chem. Rev.* **101**, 3581–3610 (2001).
13. K. L. Skubi, T. R. Blum, T. P. Yoon, Dual catalysis strategies in photochemical synthesis. *Chem. Rev.* **116**, 10035–10074 (2016).
14. B. R. McDonald, K. A. Scheidt, Intermolecular reductive couplings of arylidene malonates *via* Lewis acid/photoredox cooperative catalysis. *Org. Lett.* **20**, 6877–6881 (2018).
15. R. C. Betori, B. R. McDonald, K. A. Scheidt, Reductive annulations of arylidene malonates with unsaturated electrophiles using photoredox/Lewis acid cooperative catalysis. *Chem. Sci.* **10**, 3353–3359 (2019).
16. D. W. Robbins, J. F. Hartwig, A simple, multidimensional approach to high-throughput discovery of catalytic reactions. *Science* **333**, 1423–1427 (2011).
17. A. McNally, C. K. Prier, D. W. C. MacMillan, Discovery of an α-amino C-H arylation reaction using the strategy of accelerated serendipity. *Science* **334**, 1114–1117 (2011).
18. K. D. Collins, F. Glorius, A robustness screen for the rapid assessment of chemical reactions. *Nat. Chem.* **5**, 597–601 (2013).
19. A. Buitrago Santanilla *et al*., Organic chemistry. Nanomole-scale high-throughput chemistry for the synthesis of complex molecules. *Science* **347**, 49–53 (2015).
20. I. Sinclair *et al*., Novel acoustic loading of a mass spectrometer: Toward next-generation high-throughput MS screening. *J. Lab. Autom.* **21**, 19–26 (2016).
21. M. Wleklinski *et al*., High throughput reaction screening using desorption electrospray ionization mass spectrometry. *Chem. Sci.* **9**, 1647–1653 (2018).
22. S. Lin *et al*., Mapping the dark space of chemical reactions with extended nanomole synthesis and MALDI-TOF MS. *Science* **361**, eaar6236 (2018).
23. J. R. Cabrera-Pardo, D. I. Chai, S. Liu, M. Mrksich, S. A. Kozmin, Label-assisted mass spectrometry for the acceleration of reaction discovery and optimization. *Nat. Chem.* **5**, 423–427 (2013).
24. A. B. Diagne, S. Li, G. A. Perkowski, M. Mrksich, R. J. Thomson, Samdi mass spectrometry-enabled high-throughput optimization of a traceless Petasis reaction. *ACS Comb. Sci.* **17**, 658–662 (2015).
25. M. Mrksich, Mass spectrometry of self-assembled monolayers: A new tool for molecular surface science. *ACS Nano* **2**, 7–18 (2008).
26. M. N. Yousaf, M. Mrksich, Diels–Alder reaction for the selective immobilization of protein to electroactive self-assembled monolayers. *J. Am. Chem. Soc.* **121**, 4286–4287 (1999).
27. S. Li, M. Mrksich, An unusual salt effect in an interfacial nucleophilic substitution reaction. *Langmuir* **34**, 6713–6718 (2018).
28. K. Y. Helal, A. Alamgir, E. J. Berns, M. Mrksich, Traceless immobilization of analytes for high-throughput experiments with SAMDI mass spectrometry. *J. Am. Chem. Soc.* **140**, 8060–8063 (2018).
29. W. Chen *et al*., Building congested ketone: Substituted Hantzsch ester and nitrile as alkylation reagents in photoredox catalysis. *J. Am. Chem. Soc.* **138**, 12312–12315 (2016).
30. N. R. Patel, C. B. Kelly, M. Jouffroy, G. A. Molander, Engaging alkenyl halides with alkylsilicates *via* photoredox dual catalysis. *Org. Lett.* **18**, 764–767 (2016).
31. L. Chu, C. Ohta, Z. Zuo, D. W. C. MacMillan, Carboxylic acids as a traceless activation group for conjugate additions: A three-step synthesis of (±)-pregabalin. *J. Am. Chem. Soc.* **136**, 10886–10889 (2014).
32. T. Courant, G. Masson, Recent progress in visible-light photoredox-catalyzed intermolecular 1,2-difunctionalization of double bonds *via* an atra-type mechanism. *J. Org. Chem.* **81**, 6945–6952 (2016).
33. J. Xuan, W.-J. Xiao, Visible-light photoredox catalysis. *Angew. Chem. Int. Ed. Engl.* **51**, 6828–6838 (2012).
34. J. M. R. Narayanam, C. R. J. Stephenson, Visible light photoredox catalysis: Applications in organic synthesis. *Chem. Soc. Rev.* **40**, 102–113 (2011).
35. T. P. Yoon, M. A. Ischay, J. Du, Visible light photocatalysis as a greener approach to photochemical synthesis. *Nat. Chem.* **2**, 527–532 (2010).
36. J. W. Tucker, C. R. J. Stephenson, Shining light on photoredox catalysis: Theory and synthetic applications. *J. Org. Chem.* **77**, 1617–1622 (2012).
37. J. Luo, J. Zhang, Donor–acceptor fluorophores for visible-light-promoted organic synthesis: Photoredox/Ni dual catalytic $C(sp^3)$–$C(sp^2)$ cross-coupling. *ACS Catal.* **6**, 873–877 (2016).
38. M. H. Shaw, J. Twilton, D. W. C. MacMillan, Photoredox catalysis in organic chemistry. *J. Org. Chem.* **81**, 6898–6926 (2016).